



## Research article

# Synthesis rifaximin with copper (Rif-Cu) and copper oxide (Rif-CuO) nanoparticles Considerable dye decolorization: An application of aerobic oxidation of eco-friendly sustainable approach

Janani Mullaivendhan<sup>a</sup>, Idhayadhulla Akbar<sup>a,\*</sup>, Anis Ahamed<sup>b</sup>,  
Hissah Abdulrahman Alodaini<sup>b</sup>

<sup>a</sup> Research Department of Chemistry, Nehru Memorial College (Affiliated Bharathidasan University), Puthanampatti, 621007, Tamil Nadu, India

<sup>b</sup> Department of Botany and Microbiology, College of Science, King Saud University, P.O. Box 2455, Riyadh, 11451, Saudi Arabia

## ARTICLE INFO

**Keywords:**

Rifaximin Cu and CuO nanoparticles  
Aerobic oxidation  
Coomassie brilliant blue G250  
Rhodamine B  
Dye decolorization

## ABSTRACT

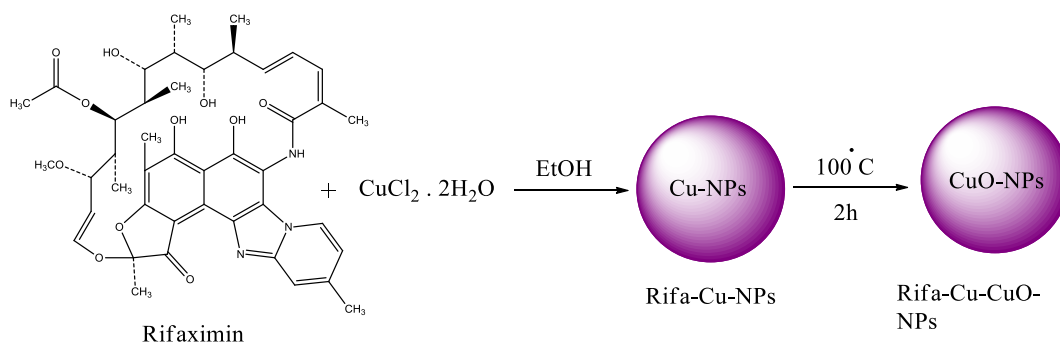
In this study, rifaximin with copper (Cu) and copper oxide (CuO) nanoparticles (NPs) were synthesised. The resultant CuO nanoparticles were used to degrade Rhodamine B (RhB) and Coomassie Brilliant Blue (G250). Rifaximin copper and copper oxide nanoparticles were characterised using Fourier-transform infrared spectroscopy (FTIR), X-ray diffraction (XRD), scanning electron microscopy (SEM), ultraviolet–visible spectroscopy (UV), X-ray Photoelectron Spectroscopy (XPS), Transmission Electron Microscopy (TEM), and gas chromatography-electrochemical mass spectrometry (GC-EI-MS). An FT-IR study confirmed the formation of Cu in the 562 cm<sup>-1</sup> peak range. Rifaximin Cu and CuO Nanoparticles displayed UV absorption peaks at 253 nm and 230 nm, respectively. Coomassie Brilliant Blue G250 was completely decolourised in Cu nanoparticles at 100 %, and Rhodamine B was also decolourised in Rifaximin CuO nanoparticles at 73 %, although Coomassie Brilliant Blue G250 Rifaximin Cu nanoparticles absorbed a high percentage of dye decolorization. The aerobic oxidation of isopropanol conversion was confirmed by GC-MS analysis. Retention time of 27.35 and 30.32 was confirmed using Cu and CuO nanoparticles as the final products of 2-propanone. It is used in the textile and pharmaceutical industries for aerobic alcohol oxidation. Rifaximin CuO nanoparticles highly active in aerobic oxidation. The novelty of this study is that, for the first time, rifaximin was used for the synthesis of copper and copper oxide nanoparticles, and it successfully achieved decolorization and aerobic oxidation.

## 1. Introduction

Rifaximin is a semisynthetic antibiotic that is derived from rifamycin and has poor gastrointestinal absorption, but exhibits excellent bactericidal activity [1]. It is commonly used to treat various conditions such as diarrhoea, irritable bowel syndrome, ulcerative colitis, and hepatic encephalopathy [2]. Rifaximin demonstrates a broad range of activity against both gram-positive and gram-negative bacteria, as well as aerobic and anaerobic microorganisms. It is believed to alter the intestinal environment [3]. Thus,

\* Corresponding author.

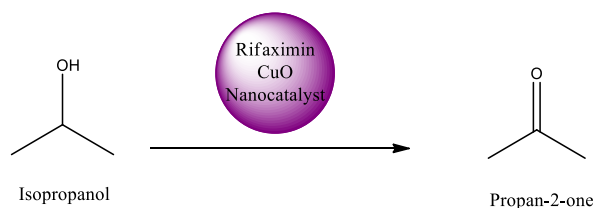
E-mail address: [a.idhayadhulla@gmail.com](mailto:a.idhayadhulla@gmail.com) (I. Akbar).



**Scheme 1.** Synthesis of Cu and CuO Nanoparticles (Rifaximin-Cu-CuO-Nanoparticles).

the RFX with the molecular formula ( $\text{C}_{43}\text{H}_{51}\text{N}_3\text{O}_{11}$ ), and chemical structure in [Scheme 1](#) is as a widely used antibiotic for treating infectious diseases, a rapid, sensitive, and selective assay is necessary for its administration [4]. In recent years, material scientists have prioritised environmentally sustainable methods for synthesising nanoscale materials [5]. The synthesis of rifaximin nanoparticles, particularly using various rifaximin solutions, is an emerging field in environmentally friendly chemistry that is believed to be simple, cost-effective, and non-toxic [6]. The use of eco-friendly products for curing and preventing human diseases has increased in recent years, attracting the attention of individuals in both developed and developing countries [7]. The widespread use of nanoparticles in various fields such as biotechnology, agriculture, chemistry, material science, energy, consumer goods, defense, optics, electronics, heavy industries, communications, medicine, microbiology, environmental remediation, and engineering is due to their unique properties [8]. Additionally, they are used in applications such as climate change, food, clothing, healthcare, treatment of lethal diseases such as cancer and respiratory infections, Alzheimer's disease [9], cosmetics, water treatment, and diagnostics [10]. Nanoparticles can be produced using various techniques, including physical, chemical, and green methods. Among these methods, green synthesis is a sustainable and cost-effective way to produce nanoparticles that does not involve the use of hazardous chemicals or high temperatures and pressures. Various types of nanoparticles, including Ag [11], Fe [12], Sb [13], Ca [14], and Au nanoparticles [15], have been synthesised using this environmentally friendly method [16]. The advantages of inorganic materials, such as copper and nickel nanoparticles, extend to energy management, textiles, batteries, healthcare, catalysis, cosmetics, semiconductors, and chemical sensing [17]. The utilisation of copper in nanostructures has gained significant interest in recent years owing to its diverse applications across various fields of science and technology [18]. Examples of oxide nanoparticles such as CuO [19], MgO [20], AgO [21], CeO<sub>2</sub> [22], ZnO [23], SnO<sub>2</sub> [24], and BaO nanoparticles [25] are highly valued for their numerous advantageous properties, including superconductivity at high temperatures, electron correlation effects, and spin dynamics, making them powerful tools in various applications. Isopropanol, also known as isopropyl alcohol (IPA), is a crucial chemical raw material and organic solvent due to its alcohol molecular structure [26,27]. It is utilised in numerous medications, serves as a solvent and chemical intermediary, and is used to produce acetone and acetone derivatives, antiseptics, food additives, cosmetics, coatings, and other products. As a volatile, colourless solvent, it is commonly referred to as 2-propanol or isopropyl alcohol [28].

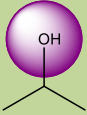
Wool fabrics are frequently dyed with water-soluble Rhodamine B dyes, which are also used in the textile industry. Rhodamine B is employed in various industries, including paper, plastics, printing, and leather, as a cosmetic, dye, photosensitizer, water tracer, paint manufacturing, food processing, fluorescent marker for microscopic structural investigations, and biological dye for biomedical research [29]. Coomassie Brilliant Blue (CBB) is a dye that is commonly used to stain proteins in a variety of electrophoretic profiles and to quantify solutions. There are two types of CBB dyes, CBB R250 and CBB G-250, which differ in the presence of additional methyl groups. The number "250" in the dye name indicates the concentration of dye, and "Coomassie" is a trademarked name owned by Imperial Chemical Industries (ICI) [30]. CBB G250 is commonly used to determine protein concentration [31]. Industrial expansion and environmental pollution have negative effects on human health, with water contamination being a serious problem, particularly in wastewater from the food, beverage, leather, cosmetic, dyeing, textile, and printing industries. Traditional wastewater treatment methods are generally insufficient for dealing with synthetic dyes, which may persist in the environment for extended periods and harm ecosystems [32]. Coomassie Brilliant Blue G250 and Rhodamine B are examples of dyes with various chemical structures. Organic compounds can be oxidised to produce the desired compounds, and oxidants are also reduced simultaneously. Aerobic oxidation is the most effective method for preventing oxidation from contaminating the environment [33]. Efficient and cost-effective catalytic systems for aerobic oxidation processes are crucial due to significant advancements in this field. However, conventional transition-metal-catalysed aerobic oxidation processes often require precise reaction conditions and expensive radical initiators [34]. Oxidation is necessary for activating and controlling radical reactions to produce oxygenated chemicals, such as ethanol, aldehydes, ketones, carboxylic acids, and epoxides from hydrocarbons [35]. Developing efficient and long-lasting catalytic processes for selective oxidation reactions is important in the pharmaceutical and chemical industries because oxidation is a common concern in the manufacturing of fine chemicals [36]. To our knowledge, the present study is the first to focus on exploiting copper and copper oxide nanoparticles to enhance the determination of rifaximin using dye decolorization and aerobic oxidation techniques.



**Scheme 2. Aerobic oxidation of Isopropanol conversion.**

**Table 1**

Reaction transformation of hydroxyl compounds used in industry.

S No	Chemical Name	Conversion of Product	Drawback
1.	 Isopropanol	 propan-2-one	<p>Accidental poisoning might result with applying a lot of IPA to the skin. Small quantities of IPA on the skin are often not harmful, but repeated skin contact can result in rashes, itching, redness, dryness, and cracking. Corrosion may result from extended skin contact.</p> <p>Ref : PubMed</p>

## 2. Materials and methods

### 2.1. Reagents and materials

All chemicals were of analytical grade and were procured from Sigma-Aldrich. A Thermo Scientific Nicolet iS5 FTIR spectrometer, with a range of  $4000\text{--}400\text{ cm}^{-1}$ , was utilised to examine all substances. PerkinElmer GCMS model Clarus SQ8 (EI) was employed to record mass spectra.

### 2.2. Preparation of rifaximin copper nanoparticles

The copper (II) chloride dehydrate (0.01 mmol) and rifaximin (0.01 mmol) both dissolve in ethanol, and the solutions are placed in a round-bottom flask. After the mixture was stirred in a magnetic stirrer for 10 min without heating, 1 mM of sodium hydroxide pellets were dissolved in ethanol, and a few drops of the NaOH solution were added. The solution turned dark green to a light blue colour at room temperature. The Cu nanoparticles solution was filtered through ethanol and dried, and the mixture was stirred again for 30 min, during which time it turned from light blue to green. This procedure resulted in the production of 183.7 mg (95 %) of Cu nanoparticles (Scheme 1).

### 2.3. Preparation of rifaximin CuO nanoparticles

Rifaximin Cu nanoparticles are heated at  $70\text{ }^{\circ}\text{C}$ . The blue colour of the Cu nanoparticles changed to that of black CuO nanoparticles. Subsequently, the mixture was cooled and collected. This procedure resulted in the production of 171.3 mg (81 %) of CuO nanoparticles (Scheme 1).

### 2.4. Aerobic oxidation of isopropanol conversion

The synthesis of Rifaximin Cu and CuO nanoparticles and the development of novel methods that use substituted aromatic

aldehydes as essential building blocks for the synthesis of molecules with a variety of functions. GC-EI-MS separation was optimised using the parameters described in the techniques section, resulting in the separation of all target components. Finally, isopropanol was completely and more quickly evaporated in 2-propanone than in various aliphatic alcohols. A recovery experiment was conducted to evaluate the stability and activity of the synthesised Rifaximin Cu and CuO nanoparticles (Scheme 2). Reaction transformations of the hydroxyl compounds used in industry (Table 1).

### 2.5. Dye decolorization of rifaximin copper and copper oxide nanoparticles

During the decolorization process, organic contaminants with vivid colours were removed from the sample mixture. When the solid product and impurities are thoroughly dissolved in a suitable solvent, this technique is typically applied in the solution phase. Analysis of decolorization activity: the dye was dissolved in water in a 5 mL volumetric flask containing 0.2 m mol/liter of each of the two different organic dyes, namely Coomassie Brilliant Blue G250 (CBBG250), and Rhodamine B. Next, 2 mg of the synthesised Cu and CuO nanoparticles was added. The sample tubes were sealed with Cu and CuO nanoparticles.

### 2.6. Characterization of copper and copper oxide nanoparticles (Cu and CuO NPs)

#### 2.6.1. Fourier transform infrared spectroscopy (FTIR)

The FTIR investigation was conducted using a KBr pellet approach with a 4000-400  $\text{cm}^{-1}$  determined spectral range using a Tensor 27 (Nicolet iS5 FT-IR KBR Windows Spectrometer from Thermo Scientific). The nanoparticles were combined to produce pellets using 2 mg dry powder and 200 mg KBr [37].

#### 2.6.2. UV-vis spectroscopy

The nanoparticles were created using a quartz cuvette and UV-Vis spectrophotometre (Optizen 3220, double beam) [38].

#### 2.6.3. X-ray Photoelectron Spectroscopy (XPS)

The X-ray photoelectron spectrometry (XPS) technique, which was coupled with an Al K X-ray light source and featured ion generators with an energy range of 100–3 K eV, was used to investigate the chemical states and surface chemistry of the elements [33].

#### 2.6.4. X-ray diffraction (XRD)

An X-ray diffractometer was used to examine the XRD patterns of Cu and CuO nanoparticles. The diffractograms were recorded using K Cu X-ray energy with Ni-filtration ( $\lambda = 1.54 \text{ \AA}$ ) at room temperature (Bruker Corp., Ettlingen, Germany, Model D8 Advance). XRD tests were performed in the 5–40  $^{\circ}2\theta$  range with 0.02  $^{\circ}2\theta$  increments [39].

#### 2.6.5. Scanning electron microscopy (SEM)

Scanning electron microscopy (MIRA3 SEM model, Tescan, Czech Republic) was employed to assess the dimensions and shape of the Cu and CuO nanoparticles. A voltage of 15 kV was used for the imaging process [40].

#### 2.6.6. Transmission electron microscopy (TEM)

The morphology, shape, and size distribution of the nanoparticles were analyzed using field-emission transmission electron microscopy (FE-TEM, FEI Tecnai F20). In the preparation method, grids covered with nickel carbon were filled with solutions containing nanoparticles from the samples and the solvent was allowed to evaporate at room temperature. The elemental makeup of the bimetallic nanoparticles was analyzed using a 200 kV ultrathin electronic window, a Genesis liquid nitrogen-cooled energy-dispersive X-ray spectroscopy (EDX) detector, and spot size of 1.2 mm and 1.7 mm for Cs and Cc, respectively [40].

#### 2.6.7. Gas chromatography and mass spectral analysis (single quadrupole GC-EI-MS)

PerkinElmer GCMS model Clarus 690-SQ8MS (EI) with EA-1 [dimethyl polysiloxane] 30 m  $\times$  0.32 mm  $\times$  0.25  $\mu\text{m}$  columns was used for the analyses. GC-EI-MS was performed using the following parameters: injection volume, 0.5  $\mu\text{L}$ , 250  $^{\circ}\text{C}$ , and 20:1 split ratio. After maintaining the temperature at 50  $^{\circ}\text{C}$  for a minute, the temperature was increased to 280  $^{\circ}\text{C}$  at 15  $^{\circ}\text{C}/\text{min}$  for 2 min. The transport gas was helium (99.9995 %) and the impact gas was nitrogen (99.999 %). Helium was used as the carrier gas, and both the transmission-line temperature and flow rate were adjusted to 1 mL/min and 250  $^{\circ}\text{C}$ , respectively. A solvent delay of 2 min was followed by a scan rate of 1500 Da/s that covered  $m/z$  15–502. The quadrupole and source had a temperature of 220  $^{\circ}\text{C}$  [33].

## 3. Result and discussion

### 3.1. FTIR analysis of rifaximin Cu and CuO nanoparticles

FT-IR spectrum analysis was used to examine the surface characteristics of rifaximin-Cu and CuO nanoparticles. To determine the contribution of rifaximin and associated functional groups to the synthesis and stability of catalysis, the FT-IR spectra of the extract before and after the creation of Cu and CuO nanoparticles were recorded. The FTIR spectra of the Cu–O and Cu–O–H samples revealed the formation of Cu nanoparticles, as evidenced by the appearance of new peaks in the absorption bands in the 3337-476  $\text{cm}^{-1}$  range. Additionally, the bending absorptions at 562  $\text{cm}^{-1}$  were attributed to bonds in the Cu nanoparticles. The infrared spectrum of

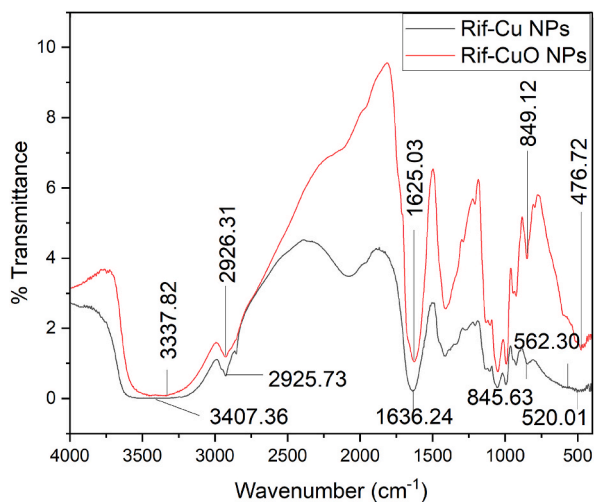


Fig. 1. FTIR spectrum of Rifaximin Cu and CuO Nanoparticles.

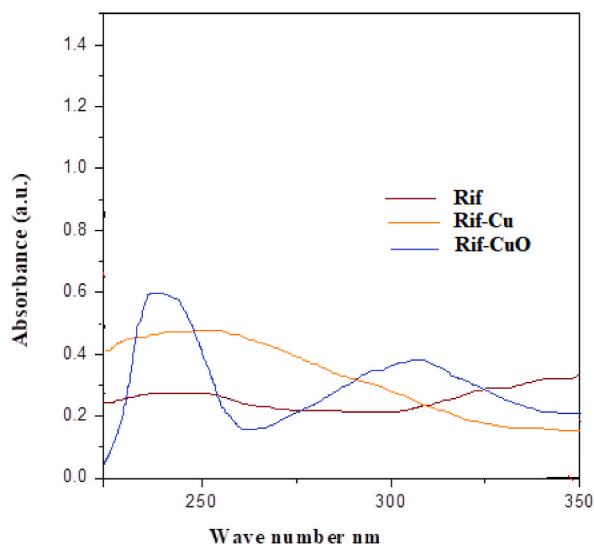


Fig. 2. UV-Vis spectra of Rifaximin Cu and CuO Nanoparticles.

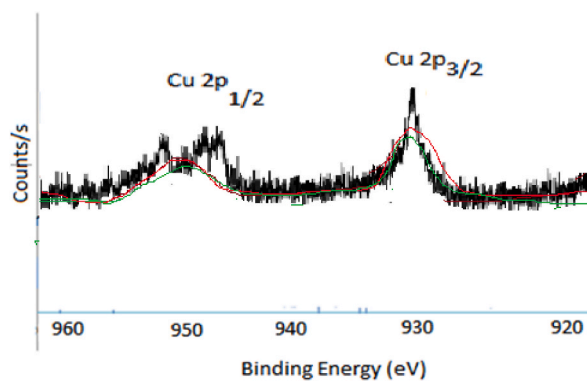


Fig. 3. Cu2p XPS ranges of Rifaximin-CuO nanoparticles.

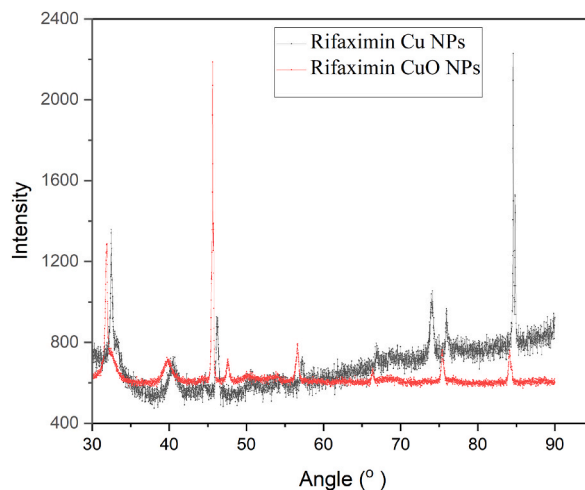


Fig. 4. XRD patterns of the Rifaximin Cu and CuO Nanoparticles.

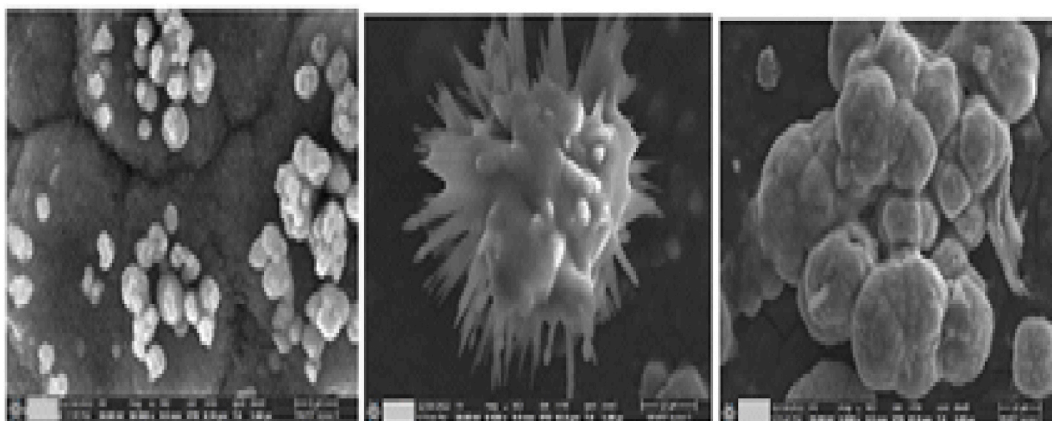


Fig. 5. SEM image of Rifaximin, Rifaximin-Cu and CuO Nanoparticles.

monoclinic CuO revealed the presence of a Cu–O bond in the range of  $520\text{ cm}^{-1}$ , while the metal-oxygen (M – O) stretching vibrations of this compound were observed at  $784$  and  $789\text{ cm}^{-1}$ . The surface of the CuO nanoparticles showed stretching and bending vibrations of water molecules and –OH group absorption peaks appearing at  $1636.2$  and  $3337.8\text{ cm}^{-1}$  (Fig. 1). The presence of copper (Cu) was verified through infrared (IR) band measurement in the range of  $550\text{--}600\text{ cm}^{-1}$  [41], while the CuO nanoparticles exhibited an absorption peak in the range of  $200\text{--}800\text{ cm}^{-1}$  [42].

### 3.2. UV-visible studies of Cu and CuO nanoparticles

UV-vis spectroscopy was used to characterise the synthesised rifaximin, Cu, and CuO nanoparticle. The UV-vis spectrum of rifaximin displays an absorption peak at  $330\text{ nm}$  [43], while Cu shows an absorption peak at  $253\text{ nm}$  [44]. The absorption peak at  $230\text{ nm}$ , attributed to the core-shell structure of the CuO nanoparticle, may be responsible for the reduced plasmon band in the bimetallic nanoparticle [45]. The UV-vis spectra of the rifaximin, Cu, and CuO nanoparticle (Fig. 2).

### 3.3. X-ray Photoelectron Spectroscopy (XPS) analysis of rifaximin CuO nanoparticles

XPS was used to analyse the surface chemistry and oxidation states of the NPs. The CuO NPs were determined to contain Cu, O, and C in the XPS survey scan; however, no other impurities were detected (Fig. 3). The XP spectra of Cu 2p electrons displayed Cu 2p<sub>3/2</sub> and Cu 2p<sub>1/2</sub> with binding energies of  $931.26$  and  $950.97\text{ eV}$ , respectively, and a spin-orbit splitting of  $19.71\text{ eV}$ . These findings correspond to the outcomes of earlier research [33].

The crystalline phase and structure of the CuO nanoparticles were analyzed using powder X-ray diffraction PXRD tests showed that the copper material produced had a cubic lattice and a zero oxidation state. XPS analysis also supported this conclusion. Based on the

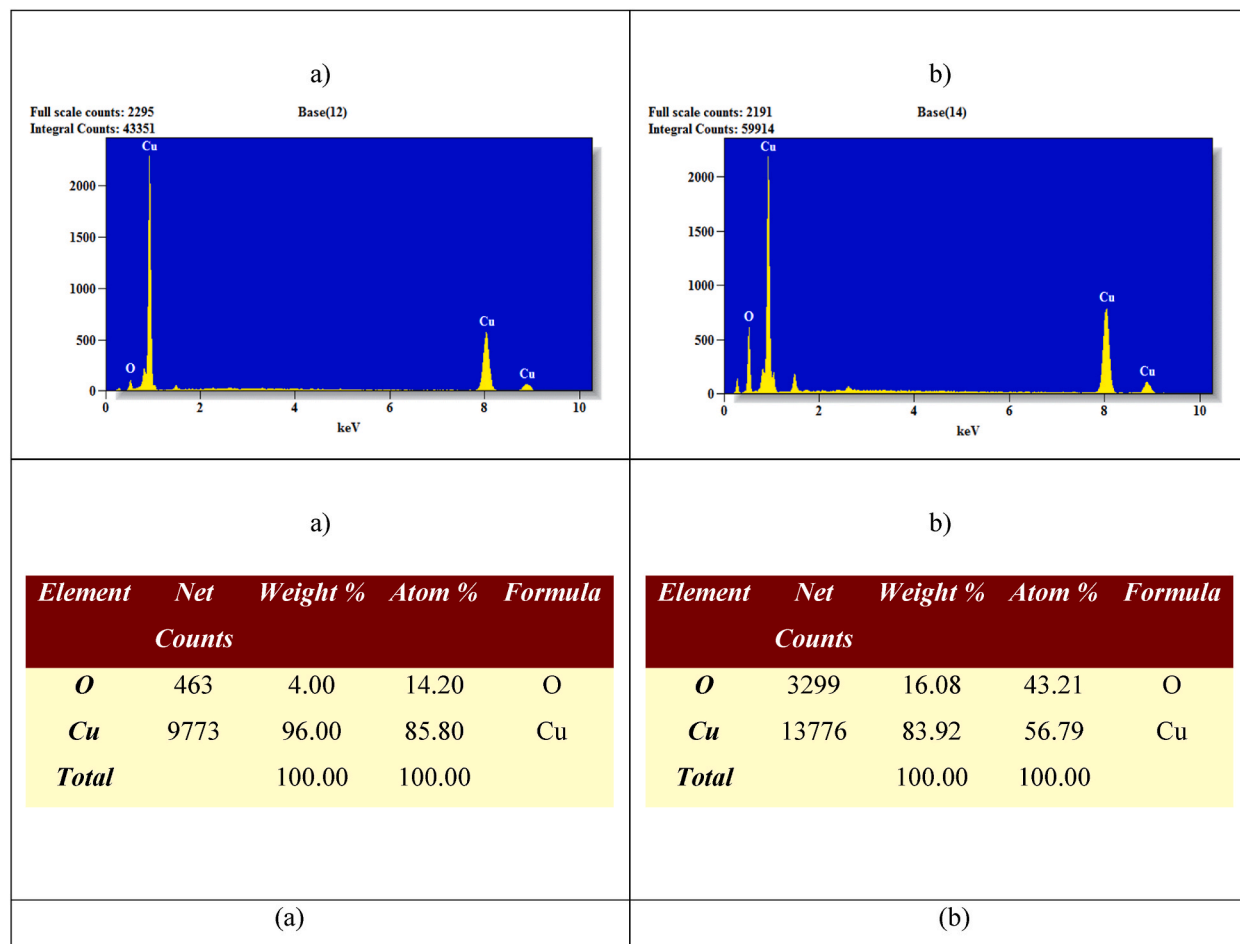


Fig. 6. EDX for Rifaximin (a) Cu nanoparticles, EDX for Rifaximin (b) CuO nanoparticles.

XRD pattern, it can be inferred that the initial formation of copper hydroxide, which was subsequently dehydrated and thermally decomposed to produce  $\text{Cu}^{2+}$  oxide, may also be due to the incorporation of  $\text{CuCl}_2$  into the CuO shell. The  $\text{Cu}^{2+}$  and CuO components contained copper without a doubt. The peak of Cu 2p<sub>3/2</sub> at 932.4 eV is due to CuO, which is most likely caused by CuO nanoparticles that are exposed to air and begin to oxidise.

### 3.4. X-ray diffraction (XRD) analysis of rifaximin Cu and CuO nanoparticles

The XRD patterns of the Cu and CuO nanoparticle displayed distinct peaks at specific angles (Fig. 4). The Cu nanoparticle exhibited peaks at 32.45°, 56.28°, 74.96°, and 80.03°, which correspond to the (110), (200), (111), and (112) planes, respectively. On the other hand, the CuO nanoparticle showed peaks at 32.46° and 56.27°, which corresponded to the (111) and (200) planes, respectively. The strong congruence between our results and the values reported in the literature for metallic copper and its face-centred cubic (FCC) structure which matched the data from standard JCPDS (No. 04–0836) [46].

### 3.5. Scanning electron microscopy (SEM) analysis of rifaximin Cu and CuO nanoparticles

The Cu and CuO nanoparticles' morphology and size were analyzed using SEM. The rifaximin were investigated using SEM at 5000 × and 30,000 × magnification, and the corresponding micrograph is displayed in (Fig. 5). The size of the nanoparticle plays a significant role in determining its characteristics and bioactivity. In this study, Rifaximin Cu nanoparticles were found to have sizes less than 10 μm and were predominantly spherical in shape [47]. The results of EDX analysis (Fig. 6a and b) revealed the presence of Cu, C, and O in the synthesised nanoparticles, with carbon (4.00 %) and copper (96.00 %) present in the Cu nanoparticle, and oxides (16.08 %) and copper (83.92 %) present in the CuO nanoparticle.

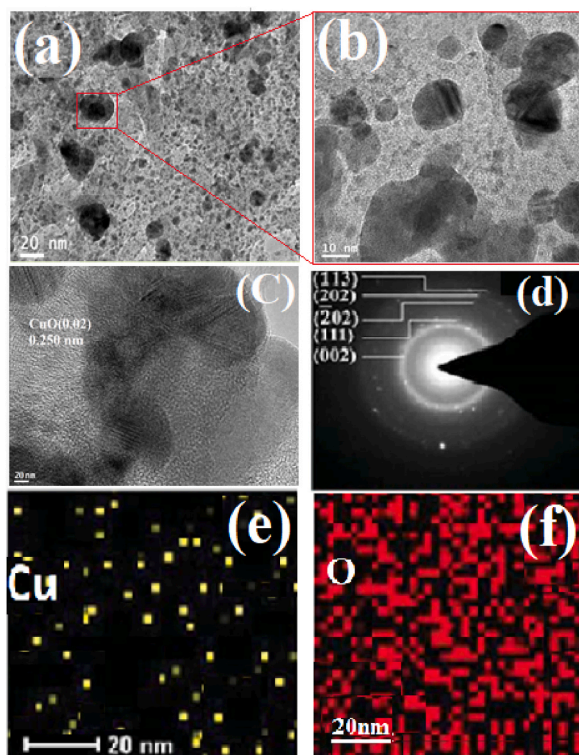
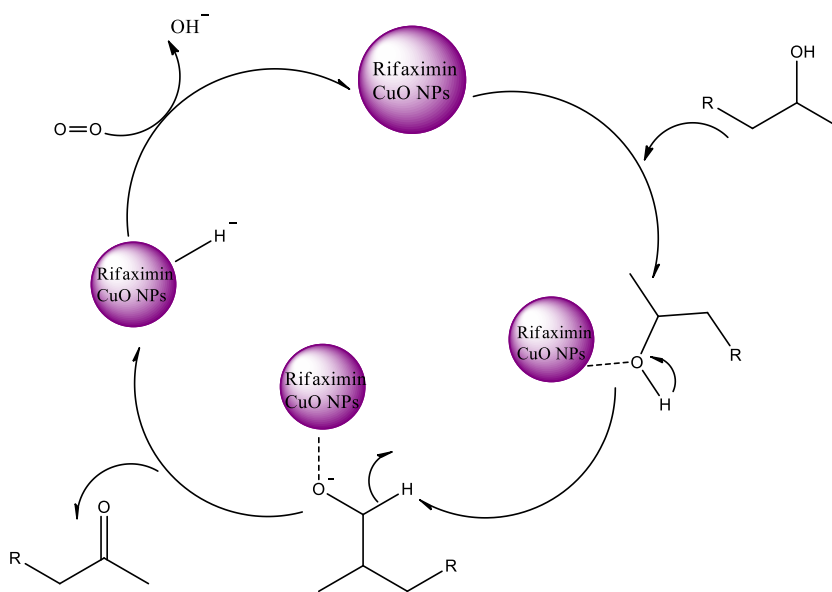


**Fig. 7.** (a) 20 nm TEM image of Rifaximin-CuO Nanoparticles, (b) HRTEM image of 5 nm (inset: FFT pattern of the matching HRTEM image), (c) Rifaximin CuO lattice fringes, (d) SAED pattern, (e) Cu  $K\alpha$  shell, and (f) O  $K\alpha$  shell.



**Scheme 3.** Mechanism for Rifaximin CuO Nanoparticles.

### 3.6. Transmission electron microscopy (TEM) analysis of rifaximin CuO nanoparticles

CuO nanoparticle morphology and surface structure examined using TEM and SAED. The CuO nanoparticle exhibited a uniform distribution (Fig. 7). The TEM image (Fig. 7a) reveals a uniform distribution of the CuO nanoparticle with a size of 10 nm (Fig. 7b). The crystal structure of CuO (002) was confirmed by the lattice fringes with a spacing of 0.250 nm that were visible in the TEM image

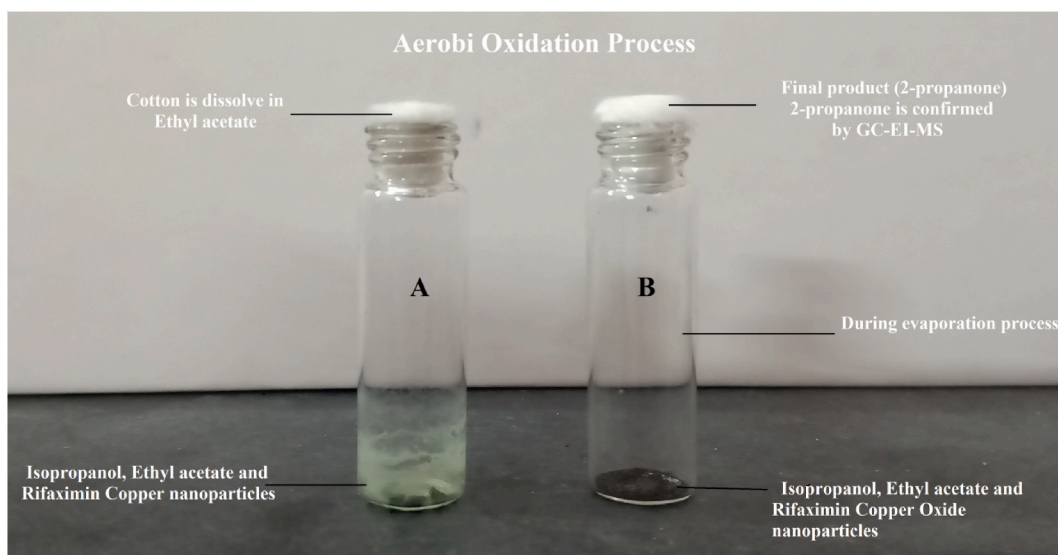


Fig. 8. Aerobic Oxidation process of Rifaximin copper and copper oxide nanoparticles.

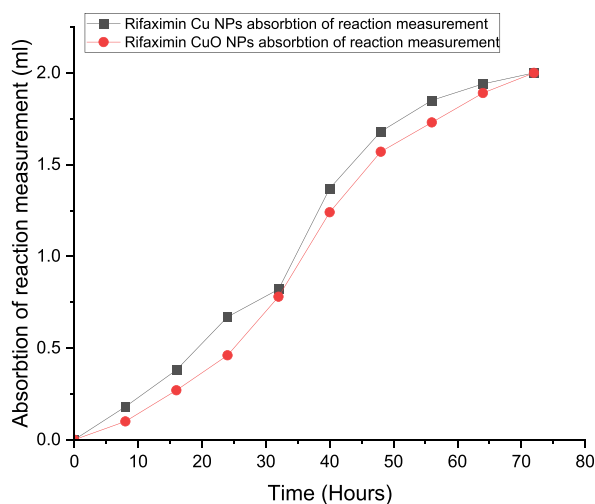


Fig. 9. Evaporation of Rifaximin Cu and CuO Nanoparticles (Aerobic oxidation).

(Fig. 7c). The SAED data (Fig. 7d) display a consecutive dotted pattern, indicating a polycrystalline structure with a face-centred cubic (FCC) arrangement. The elemental distributions of Cu and O are very similar at 10 nm (Fig. 7e and f), which also provides proof of the form of the CuO nanoparticle [48].

### 3.7. Aerobic oxidation analysis

GC separation was optimised using the parameters described in the techniques section, resulting in the separation of all target components. As part of our continued dedication to the development of unique procedures isopropanol was transformed into 2-propanone [49] with rifaximin CuO nanoparticles for numerous functions. Rifaximin-supported copper nanoparticles were successfully synthesised by transforming isopropanol into 2-propanone while maintaining the catalytic activity of the nanoparticles (Scheme 3). Various aerobic oxidation were reported in Supporting Information in (Table 1).

Cotton in a tube was used to prevent the formation of crude ethyl acetate. After a week, the crude evaporated and the volatile substance, isopropanol Rifaximin Cu and CuO nanoparticles indicated bottle A and Rifaximin CuO nanoparticles indicated bottle B. Both bottles were settled in cotton and the evaporation of Rifaximin Cu and CuO nanoparticles (aerobic oxidation) (Figs. 8 and 9). Cotton was dissolved in ethyl acetate, and the dissolved solution was injected into the GC-MS system. Retention time of 27.35 and 30.32 was confirmed by GC-EI-MS using Cu and CuO nanoparticles as the final products of 2-propanone (Figs. 10 and 11), and the

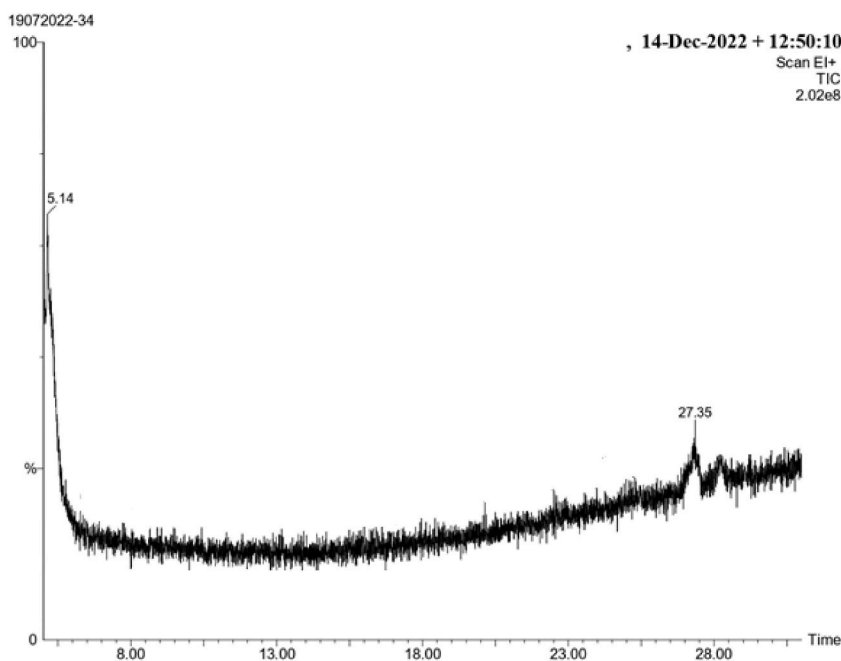


Fig. 10. GC-MS studies of aerobic oxidation of isopropanol into 2-propanone using Rifaximin- Cu nanoparticles.

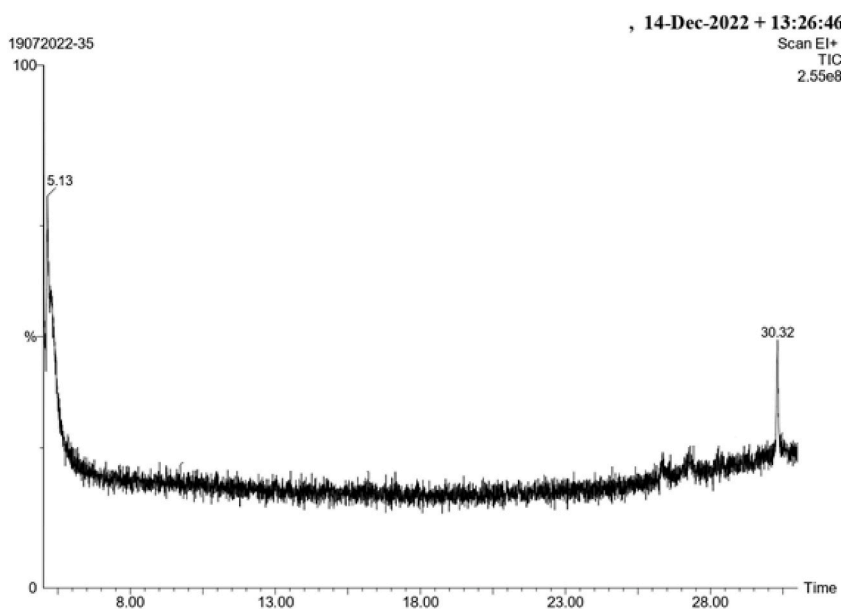


Fig. 11. GC-MS studies of aerobic oxidation of isopropanol into 2-propanone using Rifaximin- CuO nanoparticles.

appearance of a single peak in the GC chromatogram indicates that the components of the mixture, CuO nanoparticles, were completely isolated from one another. Rifaximin Cu and CuO nanoparticle were separated from the combination according to the presence of a single peak in the GC chromatogram. The molecular weight was determined by mass spectral characterisation (EI-MS), which showed a molecular ions  $m/z$  of 58.72 ( $M^+$ , 8%), which was confirmed by the molecular weight of isobutyraldehyde conforming to the molecular mass using EI-MS mass spectral analysis (Fig. 12). shows the EI-MS spectrum of 2-propanone.

### 3.8. Dye decolorization of rifaximin Cu and CuO nanoparticles

Coomassie Brilliant Blue G250 and Rhodamine B are both used in the dye decolorization process. The dye decolorization process

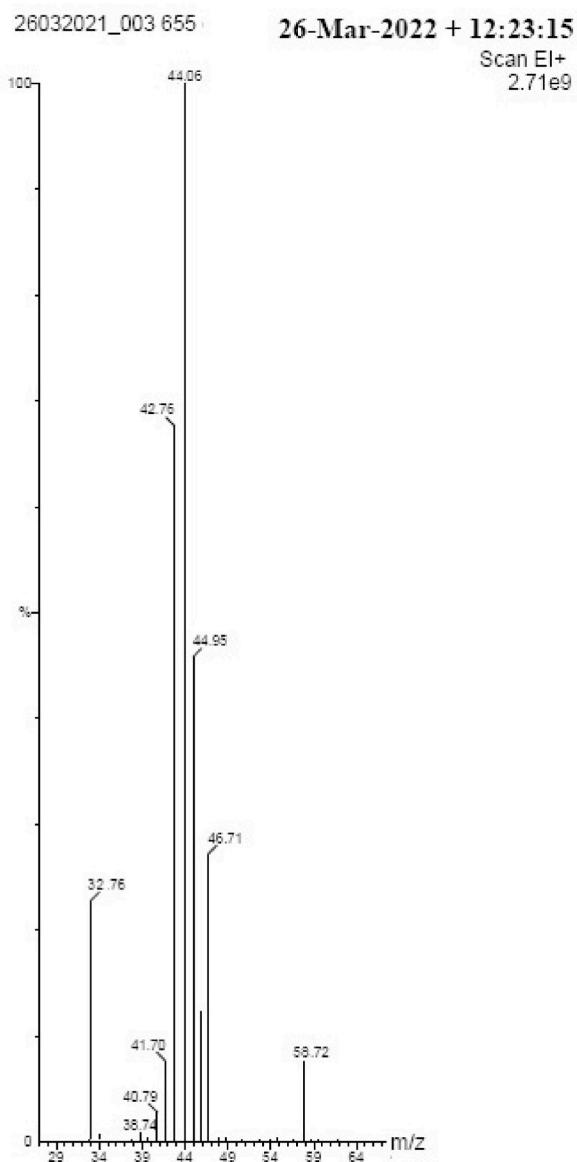


Fig. 12. Mass spectral values of 2-propanone.

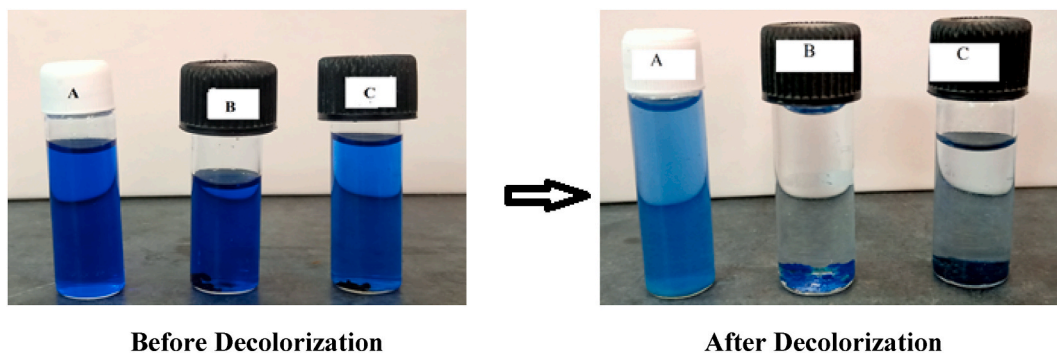
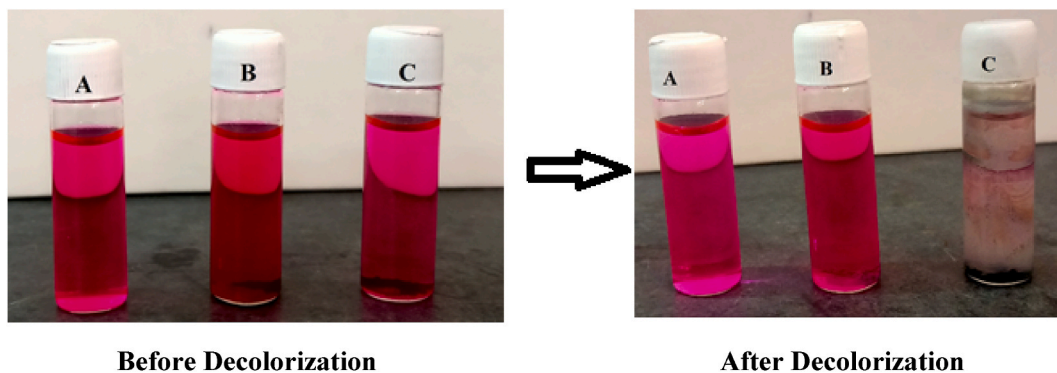
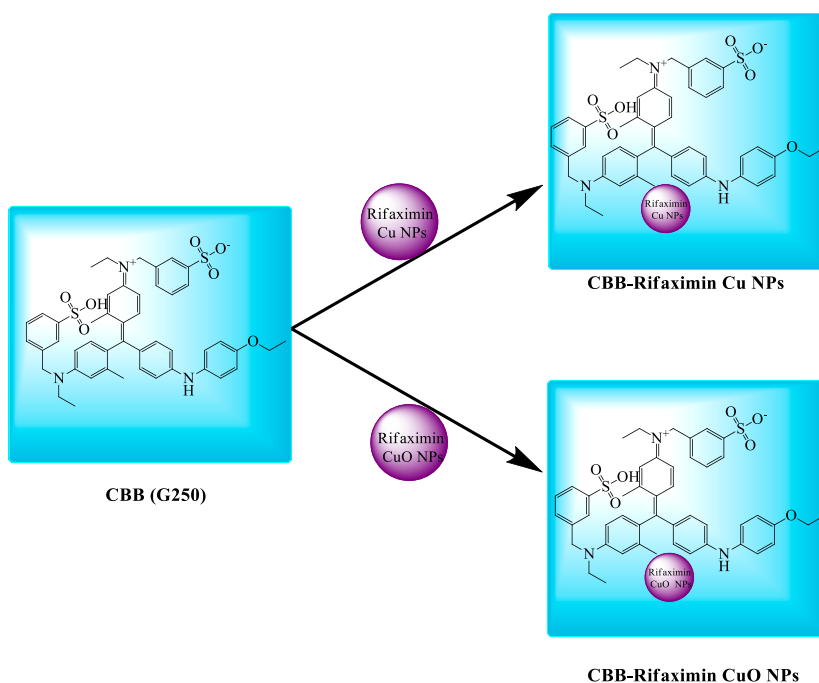


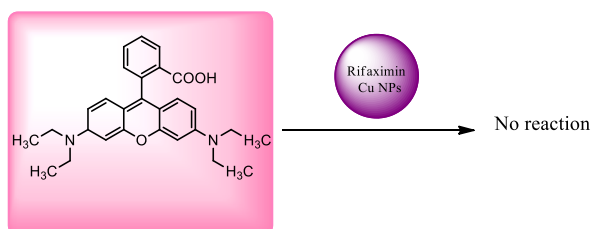
Fig. 13. Dye Decolorization: Rifaximin (A), Rifaximin Cu NPs (B) and Rifaximin CuO Nanoparticles (C) in Coomassie brilliant blue G250 Dye. (For interpretation of the references to colour in this figure legend, the reader is referred to the Web version of this article.)



**Fig. 14.** Dye decolorization: Rifaximin (A), rifaximin Cu nanoparticles (B) and rifaximin CuO nanoparticles (C) in rhodamine B dye.

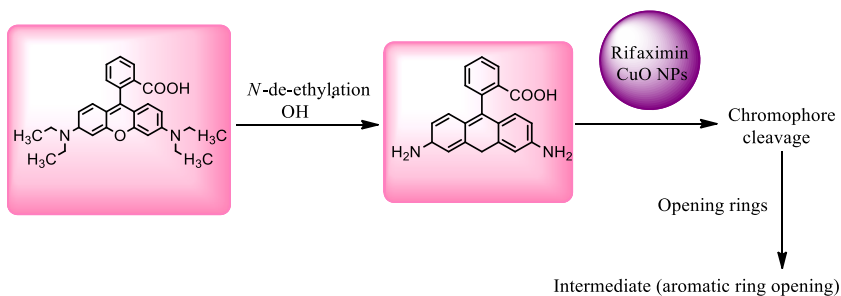


**Scheme 4.** Decolourization Rifaximin of Cu and CuO Nanoparticles in CBB G250 Dye.



**Scheme 5.** Decolorization Rifaximin of Cu Nanoparticles in Rhodamine B Dye (CuONPs).

was divided into before and after decolorization of Coomassie Brilliant Blue G250 and Rhodamine B Cu and CuO nanoparticle (Figs. 13–14). In particular, Cu nanoparticles (100 %) were highly decoloured in Brilliant Blue dye compared with the rifaximin base solution (5 %) and rifaximin-CuO nanoparticles (81 %) (Scheme 4). The synthesised rifaximin Cu and CuO nanoparticles were involved in the dye decolorization process using rhodamine B dye. After 32 h, the rifaximin CuO nanoparticles absorbed 81 % of the dye, but the Cu nanoparticles did not absorb rhodamine B dye because our Cu nanoparticles were inactive in rhodamine B dye compared with CuO



**Scheme 6.** Decolorization Rifaximin of CuO Nanoparticles in Rhodamine B Dye.

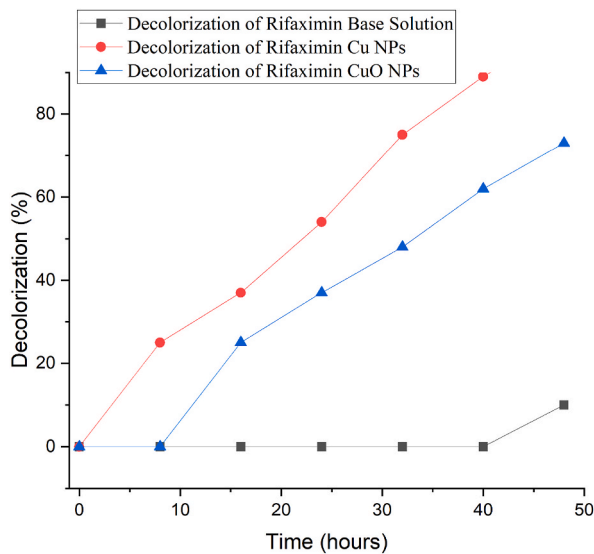


**Fig. 15.** Time-dependent dye decolorization of Coomassie Brilliant Blue G20. (For interpretation of the references to colour in this figure legend, the reader is referred to the Web version of this article.)

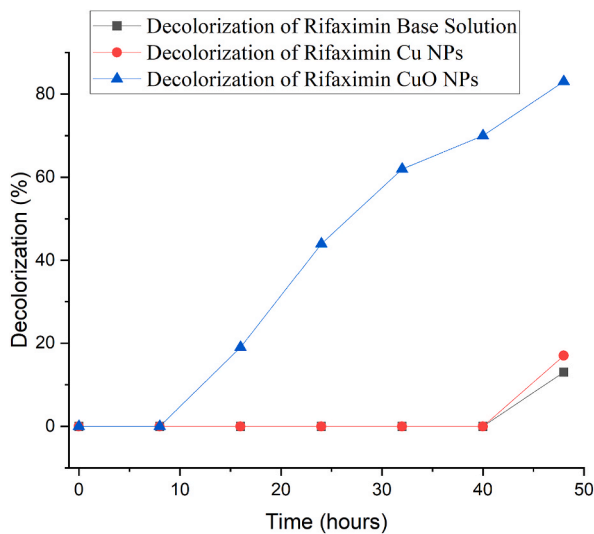


**Fig. 16.** Time-dependent dye decolorization of Rhodamine B.

nanoparticles Scheme 5 and 6. The above dye decolorization process percentage is confirmed by time-dependent dye decolorization graph (Figs. 15–16). Finally, the rifaximin-Cu nanoparticles absorb a high percentage of dye decolorization in Coomassie Brilliant Blue G250 (100 %).

#### 4. Conclusion

Investigation of rifaximin Cu and CuO nanoparticle using FT-IR, UV, SEM, TEM, XPS, XRD, and GC-EI-MS. The high purity of Rifaximin Cu nanoparticle was confirmed by XRD measurements, which revealed no extra points in the X-ray diffraction pattern. TEM images of Rifaximin CuO nanoparticle showed mostly spherical particles, 20 nm in size, with SEM images of 10 nm size. EDX analysis demonstrated 96.00 and 83.92 wt percent of the elements in the synthesised CuO nanoparticles with high Cu content. The synthesised Rifaximin Cu and CuO nanoparticles were effective in decolourising Coomassie Brilliant Blue G250 and Rhodamine B in aqueous solutions. Rifaximin Cu nanoparticle achieved complete decolorization of G250 (100 %), whereas Rhodamine B decolourised by 73 % in Rifaximin CuO nanoparticle. Comparatively, rifaximin Cu nanoparticle showed better dye decolorization due to higher dye absorption in Coomassie Brilliant Blue G250. Accordingly, rifaximin copper oxide nanoparticles have the potential to serve as a reliable, eco-friendly, and cost-effective solution for the treatment of dye-contaminated water. As a result, Rifaximin CuO nanoparticle are the best natural environmental catalyst for aerobic oxidation, and it is exhibit good catalytic performance in aerobic oxidation, are non-toxic and safe for the environment, and have a more stable recoverability. In the past, there has been no recorded application of rifaximin copper and copper oxide nanoparticles for the purposes of decolorization and aerobic oxidation. However, we successfully achieved these processes using rifaximin, copper, and copper oxide nanoparticles.

#### Data accessibility

Data will be made available upon request.

#### CRediT authorship contribution statement

**Janani Mullaivendhan:** Methodology, Formal analysis. **Idhayadhulla Akbar:** Supervision, Investigation. **Anis Ahamed:** Software, Data curation. **Hissah Abdulrahman Alodaini:** Funding acquisition.

#### Declaration of competing interest

The authors declare that they have no known competing financial interests or personal relationships that could have appeared to influence the work reported in this paper.

#### Acknowledgement

The authors thank the Department of Science and Technology, Government of India for their support under DST-FIST programme for Nehru Memorial College, Puthanampatti in Tamil Nadu, India (SR/FST/COLLEGE-372/2018). The authors are grateful to the Researchers Supporting Project number (RSP2024R479), King Saud University, Riyadh, Saudi Arabia.

#### Appendix A. Supplementary data

Supplementary data to this article can be found online at <https://doi.org/10.1016/j.heliyon.2024.e25285>.

#### References

- [1] A. Torre, J. Córdova-Gallardo, A.C. Frati Munari, Rifaximin alfa and liver diseases: more than a treatment for encephalopathy, a disease modifier, *Therapeut. Clin. Risk Manag.* (2023) 839–851, <https://doi.org/10.2147/TCRM.S425292>.
- [2] A.C. Kogawa, H.R.N. Salgado, Status of rifaximin: a review of characteristics, uses and analytical methods. *Critical Reviews in Analytical Chemistry*, *Crit. Rev. Anal. Chem.* 48 (6) (2018) 459–466, <https://doi.org/10.1080/10408347.2018.1447355>.
- [3] A.S. El-Kholany, H.A. Hafith, N.M. Gaber, Spectrophotometric and biological studies for the interaction of rifaximin with Co, Cu, Fe and vitamin, C, *J. Phys.* 2305 (1) (2022) 012039, <https://doi.org/10.1088/1742-6596/2305/1/012039>.
- [4] A.C. Kogawa, H.R.N. Salgado, Status of Rifaximin: a review of characteristics, uses and analytical methods, *Crit. Rev. Anal. Chem.* 48 (6) (2018) 459, <https://doi.org/10.1080/10408347.2018.1447355>.
- [5] A. Livingston, B.L. Trout, I.T. Horvath, M.D. Johnson, L. Vaccaro, J. Coronas, C.W. Babbitt, X. Zhang, T. Pradeep, E. Drioli, J.D., Hayler, Challenges and directions for green chemical engineering—role of nanoscale materials, *Sustainable nanoscale engineering* (2020) 1–18, <https://doi.org/10.1016/B978-0-12-814681-1.00001-1>.
- [6] D. Kumar, A. Gautam, D.K. Tripathi, K.M. Poluri, P. P., Synthesis Kundu, Characterization and biological influences of rifaximin loaded melanin/zinc oxide nanoparticles, *J. Drug Deliv. Sci. Technol.* 77 (2022) 103875, <https://doi.org/10.1016/j.jddst.2022.103875>.
- [7] Z. Gharari, P. Hanachi, H. Sadeghinia, T.R. Walker, Eco-friendly green synthesis and characterization of silver nanoparticles by *Scutellaria multicaulis* leaf extract and its biological activities, *Pharmaceuticals* 16 (7) (2023) 992, <https://doi.org/10.3390/ph16070992>.

- [8] P. Mondal, A. Anweshan, M.K. Purkait, Green synthesis and environmental application of iron-based nanomaterials and nanocomposite: a review, *Chemosphere* 259 (2020) 127509, <https://doi.org/10.1016/j.chemosphere.2020.127509>.
- [9] S. Faisal, M. Rizwan, R. Ullah, A. Alotaibi, A. Khattak, N. Bibi, M. Idrees, *Paraclostridium benzoelyticum* bacterium-mediated zinc oxide nanoparticles and their in vivo multiple biological applications, *Oxid. Med. Cell. Longev.* (2022), <https://doi.org/10.1155/2022/5994033>.
- [10] S. Shah, S.A. Shah, S. Faisal, A. Khan, R. Ullah, N. Ali, M. Bilal, Engineering novel gold nanoparticles using *Sageretia thea* leaf extract and evaluation of their biological activities, *J. Nanostructure Chem* 12 (1) (2022) 129–140, <https://doi.org/10.1007/s40097-021-00407-8>.
- [11] K. Varghese Alex, P. Tamil Pavaai, R. Rugmini, M. Shiva Prasad, K. Kamakshi, K.C. Sekhar, Green synthesized Ag nanoparticles for bio-sensing and photocatalytic applications, *ACS Omega* 5 (22) (2020) 13123–13129, <https://doi.org/10.1021/acsomega.0c01136>.
- [12] H. Liang, X. Wu, G. Zhao, K. Feng, K. Ni, X. Sun, Renal clearable ultrasmall single-crystal Fe nanoparticles for highly selective and effective ferroptosis therapy and immunotherapy, *J. Am. Chem. Soc.* 143 (38) (2021) 15812–15823, <https://doi.org/10.1021/jacs.1c07471>.
- [13] Z. Yi, N. Lin, W. Zhang, W. Wang, Y. Zhu, Qian, Preparation of Sb nanoparticles in molten salt and their potassium storage performance and mechanism, *Nanoscale* 10 (27) (2018) 13236–13241, <https://doi.org/10.1039/C8NR03829E>.
- [14] M. Golshan, S. Osfouri, R. Azin, T. Jalali, N.R. Moheimani, Efficiency and stability improvement of natural dye-sensitized solar cells using the electrospun composite of TiO<sub>2</sub> nanofibres doped by the bio-Ca nanoparticles, *Int. J. Energy Res.* 46 (11) (2022) 15407–15418, <https://doi.org/10.1002/er.8242>.
- [15] P. Suchomel, L. Kvitek, R. Prucek, A. Panacek, A. Halder, S. Vajda, R. Zboril, R. Simple size-controlled synthesis of Au nanoparticles and their size-dependent catalytic activity, *Sci. Rep.* 8 (1) (2018) 4589, <https://doi.org/10.1038/s41598-018-22976-5>.
- [16] T. Hussain, S. Faisal, M. Rizwan, N. Zaman, M. Iqbal, A. Iqbal, Z. Ali, Green synthesis and characterization of copper and nickel hybrid nanomaterials: investigation of their biological and photocatalytic potential for the removal of organic crystal violet dye, *J. Saudi Chem. Soc.* 26 (4) (2022) 101486, <https://doi.org/10.1016/j.jscs.2022.101486>.
- [17] S. Faisal, N.S. Al-Raddadi, H. Jan, S.A. Abdullah, Shah, S. Shah, M. Rizwan, Z. Afsheen, Z. Hussain, M.N. Uddin, M. Idrees, Curcuma longa mediated synthesis of copper oxide, nickel oxide and Cu-Ni bimetallic hybrid nanoparticles: characterization and evaluation for antimicrobial, anti-parasitic and cytotoxic potentials, *Coatings* 11 (7) (2021) 849, <https://doi.org/10.3390/coatings11070849>.
- [18] A.D. Kute, R.P. Gaikwad, I.R. Warkad, M.B. Gawande, A review on the synthesis and applications of sustainable copper-based nanomaterials, *Green Chem.* 24 (9) (2022) 3502–3573, <https://doi.org/10.1039/D1GC04400A>.
- [19] S. Faisal, H. Jan, Abdullah, I. Alam, M. Rizwan, Z. Hussain, K. Sultana, Z. Ali, M.N. Uddin, In vivo analgesic, anti-inflammatory, and anti-diabetic screening of *Bacopa monnieri*-synthesized copper oxide nanoparticles, *ACS Omega* 7 (5) (2022) 4071–4082, <https://doi.org/10.1021/acsomega.1c05410>.
- [20] M.A. Khan, F. Ali, S. Faisal, M. Rizwan, Z. Hussain, N. Zaman, Z. Afsheen, M.N. Uddin, N. Bibi, Exploring the therapeutic potential of *Hibiscus rosa sinensis* synthesized cobalt oxide (Co<sub>3</sub>O<sub>4</sub>-NPs) and magnesium oxide nanoparticles (MgO-NPs), *Saudi J. Biol. Sci.* 28 (9) (2021) 5157–5167, <https://doi.org/10.1016/j.sjbs.2021.05.035>.
- [21] S.S. Mughal, S.M. Hassan, Comparative study of AgO nanoparticles synthesized via biological, chemical and physical methods, A review, *J. Mater. Sci.* 7 (2) (2022) 15–28.
- [22] H. Jan, M.A. Khan, H. Usman, M. Shah, R. Ansari, S. Faisal, N. Ullah, L. Rahman, The *Aquilegia pubiflora* (Himalayan columbine) mediated synthesis of nanoceria for diverse biomedical applications, *RSC Adv.* 10 (33) (2020) 9219–19231, <https://doi.org/10.1039/D0RA01971B>.
- [23] S. Faisal, H. Jan, S.A. Shah, S. Shah, A. Khan, M.T. Akbar, M. Rizwan, F. Jan, Wajidullah, N. Akhtar, A. Khattak, Green synthesis of zinc oxide (ZnO) nanoparticles using aqueous fruit extracts of *Myristica fragrans*: their characterizations and biological and environmental applications, *ACS Omega* 6 (14) (2021) 9709–9722, <https://doi.org/10.1021/acsomega.1c00310>.
- [24] M. Rizwan, S. Faisal, M.H. Tariq, S. Zafar, A. Khan, F. Ahmad, Enterobacter hormaechei-driven novel biosynthesis of tin oxide nanoparticles and evaluation of their anti-aging, cytotoxic, and enzyme inhibition potential, *ACS Omega* 8 (30) (2023) 27439–27449, <https://doi.org/10.1021/acsomega.3c02932>.
- [25] A. U. Rahman Abdullah, S. Faisal, M.M. Almostafa, N.S. Younis, G. Yahya, Multifunctional spirogyra-hyalina-mediated barium oxide nanoparticles (BaONPs): synthesis and applications, *Mol* 28 (17) (2023) 6364, <https://doi.org/10.3390/molecules28176364>.
- [26] K. Gosse, A. Ehrmann, Influence of FTO glass cleaning on DSSC performance, *Optik* 183 (2019) 253–256, <https://doi.org/10.1016/j.ijleo.2019.02.041>.
- [27] C. Li, P. Cheng, K. Shen, T. Zhang, X. Cao, B. Wang, B.S. Hsiao, Integrated polyamide thin-film nanofibrous composite membrane regulated by functionalized interlayer for efficient water/isopropanol separation, *J. Membr. Sci.* 553 (2018) 70–81, <https://doi.org/10.1016/j.memsci.2018.02.013>.
- [28] A. Iriondo, I. Agirre, N. Viar, J. Requies, Value-added bio-chemicals commodities from catalytic conversion of biomass derived furan-compounds, *Catal* 10 (8) (2020) 895, <https://doi.org/10.3390/catal10080895>.
- [29] M.S. Çelik, S.A. Çetinus, A.F. Yenidünya, S. Çetinkaya, B. Tüzün, Biosorption of Rhodamine B dye from aqueous solution by *Rhus coriaria* L. plant: equilibrium, kinetic, thermodynamic and DFT calculations, *J. Mol. Struct.* 1272 (2023) 134158, <https://doi.org/10.1016/j.molstruc.2022.134158>.
- [30] H.K. Ibrahim, M.A. Amy, E.T. Kreem, Decolorization of Coomassie brilliant blue G-250 dye using snail shell powder by action of adsorption processes, *RJPT* 12 (10) (2019) 4921–4925, <https://doi.org/10.5958/0974-360x.2019.00853.9>.
- [31] I. Yamaguchi, I.M. Tariqul, &A. Wang, Conjugated polymers with anionic dyes: synthesis, properties, and sensing ability for nucleosides, DNA, and BSA, *J. Appl. Polym. Sci.* 138 (33) (2021) 50810, <https://doi.org/10.1002/app.50810>.
- [32] A. Mancuso, N. Blangetti, O. Sacco, F.S. Freyria, B. Bonelli, S. Esposito, V. Vaiano, Photocatalytic degradation of crystal violet dye under visible light by Fe-doped TiO<sub>2</sub> prepared by reverse-micelle sol-gel method, *J. Nanomater.* 2 (2023) 270, <https://doi.org/10.3390/nano13020270>.
- [33] A. Mani, A. Ahmed, M.A. El-Sheikh, I. Akbar, Natural dried Vanilla Beans powder (VBP) mediated CuO nanoparticles catalysis: aerobic oxidation of hydroxylamines from industrial waste water using ecofriendly method, *Ind. Crops Prod.* 191 (2023) 115915, <https://doi.org/10.1016/j.indcrop.2022.115915>.
- [34] X. Pi, Y. Feng, X. Pi, Y. Song, Z. Xu, Z. Li, W. Lin, Integration of earth-abundant photosensitizers and catalysts in metal-organic frameworks enhances photocatalytic aerobic oxidation, *ACS Catal.* 11 (3) (2021) 1024–1032, <https://doi.org/10.1021/acscatal.0c05053>.
- [35] H. Wilkes, R. Jarling, J. Schwarzbauer, Hydrocarbons and lipids: an introduction to structure, physicochemical properties, and natural occurrence. *Hydrocarbons, Oils and Lipids, Diversity, Origin, Chemistry and Fate* (2020) 3–48, <https://doi.org/10.1007/978-3-319-90569-334>.
- [36] W. Zhang, W. B. Cue, Green Techniques for Organic Synthesis and Medicinal Chemistry, *JWS*, 2018, [https://doi.org/10.1002/9781119288152\\_19](https://doi.org/10.1002/9781119288152_19).
- [37] K. Raghavanpillai Sabu, S. Sugathan, A. Idhayadhulla, M. Woldemariam, A. Akhlu, G. Biresaw, B. Tsegaye, A. Manilal, Antibacterial, antifungal, and cytotoxic activity of *Excoecaria agallocha* leaf extract, *J. Exp. Pharmacol.* (2022) 17–26, <https://doi.org/10.2147/JEP.S339383>.
- [38] A. Idhayadhulla, A. Manilal, A. Ahmed, S. Alarifi, G. Raman, Potato peels mediated synthesis of Cu (II)-nanoparticles from tyrosinase reacted with bis-(N-aminoethylethanolamine)(tyr-Cu (II)-AEEA NPs) and their cytotoxicity against Michigan cancer foundation-7 breast cancer cell line, *Mol* 26 (21) (2021) 6665, <https://doi.org/10.3390/molecules26216665>.
- [39] C. SathishKumar, R. Surendrakumar, G. Raman, D. Ali, S. Alarifi, A. Idhayadhulla, Bis-(N-aminoethylethanolamine)-Copper (II) nanocatalysis (AEEA-Cu (II)-NPs) mediated synthesis a series of 2-thioxo-1, 2, 3, 4-tetrahydropyrimidine-5-carboxamide derivatives: characterization of theoretical, computational and evaluation of molecular docking, and cytotoxicity activities, *J. King Saud Univ. Sci.* 34 (3) (2022) 101872, <https://doi.org/10.1016/j.jksus.2022.101872>.
- [40] R. Surendrakumar, A. Idhayadhulla, A. Ahmed, H.A. Alodaini, R. Gurusamy, Vermiremediation: analysis of contaminated diesel in soil using *Eisenia fetida* and ZnO nanoparticles with cow dung, *Front. Environ. Sci.* 10 (2022) 934287, <https://doi.org/10.3389/fenvs.2022.934287>.
- [41] M. Khodaie, N. Ghasemi, Green synthesis and characterization of copper nanoparticles using *Eryngium campestre* leaf extract, *Bulg. Chem. Commun.* 50 (2018) 244–250.
- [42] A.D. Khalaji, Z. Pazhand, K. Kiani, P. Machek, M. Jarosova, R. Mazandarani, CuO nanoparticles: preparation, characterization, optical properties, and antibacterial activities, *J. Mater. Sci. Mater.* 31 (2020) 11949–11954, <https://doi.org/10.1007/s10854-020-03749-1>.
- [43] H. Noor, I.G. David, M.L. Jinga, D.E. Popa, M. Buleandra, E.E. Iorgulescu, A.M. Ciobanu, State of the art on developments of (bio) sensors and analytical methods for rifamycin antibiotics determination, *Sensors* 23 (2) (2023) 976, <https://doi.org/10.3390/s23020976>.
- [44] B. Vyhldalová, P. Pečinková, H. Li, P. Anzenbacher, A. Špičáková, E. Anzenbacherová, V. Chow, J. Liu, H. Krause, D.J. Wilson, and T. Berés, In Vitro Safety Signals for Potential Clinical Development of the Anti-inflammatory Pregnane X Receptor Agonist FKK6.

- [45] K.S. Siddiqi, A. Husen, Current status of plant metabolite-based fabrication of copper/copper oxide nanoparticles and their applications: a review, *iomater. Res.* 24 (1) (2020) 1–15, <https://doi.org/10.1186/s40824-020-00188-1>.
- [46] D. Mardiansyah, T. Badloe, K. Triyana, M.Q. Mehmood, N. Raeis-Hosseini, Y. Lee, H. Sabarman, K. Kim, J. Rho, Effect of temperature on the oxidation of Cu nanowires and development of an easy to produce, oxidation-resistant transparent conducting electrode using a PEDOT: PSS coating, *Sci. Rep.* 8 (1) (2018) 10639, <https://doi.org/10.1038/s41598-018-28744-9>.
- [47] S.A. Algharib, A. Dawood, K. Zhou, D. Chen, C. Li, K. Meng, A. Zhang, W. Luo, S. Ahmed, L. Huang, S. Xie, Preparation of chitosan nanoparticles by ionotropic gelation technique: effects of formulation parameters and in vitro characterization, *J. Mol. Struct.* 1252 (2022) 132129, <https://doi.org/10.1016/j.molstruc.2021.132129>.
- [48] R. BoopathiRaja, M. Parthivarman, A.N. Begum, Hydrothermal induced novel CuCo<sub>2</sub>O<sub>4</sub> electrode for high performance supercapacitor applications, *Vacuum* 165 (2019) 96–104, <https://doi.org/10.1016/j.vacuum.2019.04.013>.
- [49] A. Aitlaalim, F. Ouanji, A. Benzaouak, M. Kacimi, M. Ziyad, L.F. Liotta, Preparation, characterization and catalytic activity in 2-propanol conversion of potassium and antimony mixed oxides, *Top. Catal.* 63 (2020) 1388–1397, <https://doi.org/10.1007/s11244-020-01370-4>.